# Analyst

## Accepted Manuscript

This article can be cited before page numbers have been issued, to do this please use: S. Sass, W. F.M. Stöcklein, A. Klevesath, J. Hurpin, M. Menger and C. Hille, *Analyst*, 2019, DOI: 10.1039/C9AN01247H.




ROYAL SOCIETY OF CHEMISTRY

rsc.li/analyst

Analyst

View Article Online
DOI: 10.1039/C9AN01247H

PAPER

# Binding affinity data of DNA aptamers for therapeutic anthracyclines from microscale thermophoresis and surface plasmon resonance spectroscopy†

Received 00th January 20xx,
Accepted 00th January 20xx

DOI: 10.1039/x0xx00000x

www.rsc.org/

Stephan Sass,[a] Walter F.M. Stöcklein,[b] Anja Klevesath,[b] Jeanne Hurpin,[a] Marcus Menger*‡[b] and Carsten Hille*‡[a,c]

Anthracyclines like daunorubicin (DRN) and doxorubicin (DOX) play an undisputed key role in cancer treatment, but their chronic administration can cause severe side effects. For precise anthracycline analytical systems, aptamers are preferable recognition elements. Here, we describe the detailed characterisation of a single-stranded DNA aptamer DRN-10 and its truncated versions for DOX and DRN detection. Binding affinities were determined from surface plasmon resonance (SPR) and microscale thermophoresis (MST) and combined with conformational data from circular dichroism (CD). Both aptamers displayed similar nanomolar binding affinities to DRN and DOX, even though their rate constants differed as shown by SPR recordings. SPR kinetic data unravelled a two-state reaction model including a 1:1 binding and a subsequent conformational change of the binding complex. This model was supported by CD spectra. In addition, the dissociation constants determined with MST were always lower than that from SPR, and especially for the truncated aptamer they differed by two orders of magnitude. This most probably reflects the methodological difference, namely labelling for MST *vs.* immobilisation for SPR. From CD recordings, we suggested a specific G-quadruplex as structural basis for anthracycline binding. We concluded that the aptamer DRN-10 is a promising recognition element for anthracycline detection systems and further selected aptamers can be also characterised with the combined methodological approach presented here.

## Introduction

The specific interaction between molecules plays a key role in almost all cellular processes such as metabolism, transport, signal transduction or structural organisation.[1] In diagnostics, these interactions are usually the basis of biosensors detecting a target molecule via a binding step to a recognition element.[2] Thus, for a comprehensive understanding of cellular processes and potential dysfunctions as well as disease treatment, interaction analysis methods are of particular interest. A bimolecular interaction can be analysed by measuring the rate constants of association and dissociation ($k_{+1}$, $k_{-1}$), the dissociation constant ($K_D$) or thermodynamic parameters ($\Delta G$, $\Delta H$, $\Delta S$). For this, a number of techniques have been established nowadays. Biochemical methods include e.g. enzyme-linked immunosorbent assay (ELISA) and co-immunoprecipitation, whereas biophysical methods comprise for instance fluorescence polarisation, surface plasmon resonance (SPR), isothermal titration calorimetry (ITC) and microscale thermophoresis (MST).[3–6] The determination of several interaction parameters is favourable, but this can lead to complex and time-consuming experiments. In many cases, evaluation of bimolecular interactions can be sufficiently and more easily performed by only measuring $K_D$. However, all available methods have their own limitations such as requirement of sample purification, fluorescence labelling or immobilisation of one interaction molecule and large size differences of the interaction molecules. Considering these reasons, one rather determines an apparent value of $K_D$, which depends on the particular method used and can vary between different ones. Thus, application of several methods is meaningful, but the results should be then discussed under the methodological point of view.

Aptamers are single-stranded RNA and DNA nucleotides, which are generated using an iterative *in vitro* selection procedure (SELEX) and bind to target molecules with high specificity and high affinity due to their specific tertiary structures.[7–9] In comparison to antibodies, aptamers possess several advantages such as fast chemical synthesis, high stability, and high chemical modification potential as well as small size. Thus, aptamers are preferable interaction molecules for different fields of research. Therefore, aptamers can be applied as recognition elements in electrochemical or optical

[a] Physical Chemistry / ALS ComBi, Institute of Chemistry, University of Potsdam, 14476 Potsdam, Germany.
[b] Fraunhofer Institute for Cell Therapy and Immunology, Branch Bioanalysis and Bioprocesses (IZI-BB), 14476 Potsdam, Germany.
E-mail: marcus.menger@izi-bb.fraunhofer.de; Tel: +49 331 58187316
[c] Technical University of Applied Sciences Wildau, 15745 Wildau, Germany.
E-mail: carsten.hille@th-wildau.de; Tel.: +49 3375 508793
†Electronic supplementary information (ESI) available.
See DOI: 10.1039/x0xx00000x
‡ These authors contributed equally.

biosensors (so-called aptasensors) for *in vitro* diagnostics, as markers for tissue imaging applications, for targeted drug delivery systems or even as therapeutic drugs.[10–12] The $K_D$-values of aptamers are typically in the pM-µM range[13], and to use aptamers in the defined application, the $K_D$-values have to be determined with the above-mentioned methods.

Anthracyclines such as daunorubicin and doxorubicin are key chemotherapeutic substances in cancer treatment since decades.[14] They intercalate into the DNA double helix inhibiting DNA duplication and transcription to mRNA and thus, inhibiting the proliferation of cancer cells.[15] Anthracyclines also appear to inhibit DNA repair resulting in DNA fragmentation. However, their chronic administration can induce severe side effects.[16] The development of new nanocarriers for targeted drug delivery could probably minimise these side effects,[17] and aptamers seem to be favourable molecular targeting agents.[18,19]

Here, we present precise binding properties of a single-stranded DNA aptamer, which has been previously generated against daunorubicin.[20] The aptamer showed an up to 1,000-fold higher binding affinity to both daunorubicin and doxorubicin than unspecific double-stranded DNA.[21,22] It has already been used in various analytical applications over the last decade. Its cooperative effects were used for binding improvement of the drug target[23,24] and its intrinsic DNAzyme activity was considered for a colorimetric assay development.[25] Particularly, the aptamer has been applied in different aptasensor types for environmental analysis[26,27] and *in vivo* real-time measurements for drug monitoring in cancer therapy.[28,29] From all selected aptamers, a 80 nt aptamer (DRN-10) and a 41 nt truncated aptamer (DRN-10v) had been analysed by SPR yielding rate constants from which $K_D$-values were calculated to be 20 nM and 272 nM, respectively.[20] However, the specificity to other anthracyclines had been only estimated from competition fluorescence assays. In this study, we have expanded the SPR studies of the daunorubicin-specific aptamer to other antibiotics. Although SPR is a label-free, real-time method allowing kinetic measurements, the immobilisation of one binding partner and rebinding or nonspecific binding at the surface can influence the measurements.[30] Therefore, the SPR-based results were compared with results from MST measurements, in which the binding of two partners is recorded in free solution.[31,32]

## Experimental

### DNA oligonucleotides and sample preparation

The single-stranded DNA oligonucleotides were synthesised by the Fraunhofer Institute for Cell Therapy and Immunology IZI-BB (Potsdam, Germany). The sequences of the oligonucleotides are: daunorubicin aptamer DRN-10 (80 nt): 5'-GGG AAT TCG AGC TCG GTA CCA TCT GTG TAA GGG GTA AGG GGT GGG GGT GGG TAC GTC TAG CTG CAG GCA TGC AAG CTT GG-3'; truncated daunorubicin aptamer DRN-10R (60 nt): 5'-GGG AAT TCG AGC TCG GTA CCA TCT GTG TAA GGG GTA AGG GGT GGG GGT GGG TAC GTC TAG-3'; further shortened daunorubicin aptamer DRN-10v (41 nt): 5'-ACC ATC TGT GTA AGG GGT AAG GGG TGG GGG TGG GTA CGT CT-3'; control Con1 (80 nt): 5'-GGG AAT TCG AGC TCG GTA CCG GCT GCT TTG CTG CAG ATT TGT GGG TGG GTG GGT GGT GAT CTG CAG GCA TGC AAG CTT GG-3'; control Con2 (79 nt): 5'-GGG AAT TCG AGC TCG GTA CCG TAC AGT ACT GCA TAT CTC ATA CTT CCT AGA TAC CAT CCC TGC AGG CAT GCA AGC TTG G-3'. All oligonucleotides were labelled with the red fluorescent dye Cy5 at the 5'-end without additional linker for MST recordings. For SPR and CD spectroscopic measurements, the oligonucleotides were used without Cy5-labelling. All oligonucleotides were delivered at 100 µM in bidest. water and stored at -20 °C.

The anthracyclines daunorubicin (DRN) and doxorubicin (DOX) as well as the antibiotics chloramphenicol (CAM) and tetracycline (TET), all from Sigma-Aldrich (Munich, Germany), were dissolved in DMSO to 20 mM and stored at 4 °C. For SPR recordings, the anthracyclines DRN and DOX were dissolved freshly in bidest. water to 10 mM stock solution, stored at 4 °C and were diluted up to 10 nM in HBS-P running buffer (10 mM HEPES, 150 mM NaCl, 0.005% (v/v) Surfactant P20, pH 7.4; GE Healthcare Europe).

For MST and SPR measurements, the oligonucleotides (aptamers and controls) were dissolved in an aptamer binding buffer consisting of 140 mM NaCl, 5 mM KCl, 1 mM $MgCl_2$, 1 mM $CaCl_2$ and 0.05% (v/v) Tween 20, 20 mM Tris-HCl, pH 7.4 (with the exception of 0.0005% (v/v) Tween 20 for SPR recordings). For activation, 1 -10 µM of aptamers were heated to 90 °C for 3 min and immediately chilled on ice for 5 min. Activated aptamers were stored at 25 °C and diluted up to 4 nM immediately in aptamer binding buffer before MST and SPR recordings. From the anthracyclines, a 1:1 dilution series could be prepared in micro-reaction tubes starting at the highest concentration of 1-10 µM. The dye-labelled aptamer concentration was kept constant in each tube at 2 nM.

For CD measurements, aptamers were used at concentrations of 15 µM in minimal buffer consisting of 10 mM Tris-HCl and 0.05% (v/v) Tween 20, pH 7.4. In addition, NaCl, KCl, $MgCl_2$ and $CaCl_2$ were added to the indicated levels and choline chloride was used to maintain ionic strength. Aptamers were heated to 90 °C for 3 min and immediately chilled on ice for 5 min before obtaining the CD spectra.

### Microscale thermophoresis

The MST measurements were performed using a Monolith NT.115 $^{Pico}$ device with nano-blue and pico-red detection channels (NanoTemper Technologies, Munich, Germany). In this device, an infrared (IR)-laser beam for inducing a temperature gradient of 2-6 K within the sample volume as well as the fluorescence excitation light were coupled with a dichroic mirror and focused on the sample. Here, the fluorescence was excited at $\lambda_{ex}$ = 620 nm ± 25 nm and fluorescence emission was detected at $\lambda_{em}$ = 690 nm ± 30 nm. For all experiments MST-grade standard treated capillaries were used, since no molecule sticking at the glass surface could be observed from the capillary scans. The capillaries



 

View Article Online
DOI: 10.1039/C9AN01347H



were filled with the sample of less than 10 µL. The MST parameter were set to red-LED power 5-20%, MST laser power 40% and the time windows of 5 s before IR-laser, 30 s during IR-laser and 5 s after IR-laser. The temperature of the instrument was set to 22 °C for all measurements. After recording the MST time traces, data were analysed using the temperature jump and the thermophoresis effect. Thus, the total fluorescence intensity was calculated for the period before starting the IR-laser ($F_{cold}$) and at the end of the IR-laser period ($F_{hot}$). From this, the normalised fluorescence $F_{norm}$ could be plotted against the ligand concentration according to Equation 1:

$$F_{norm} = (^{F_{hot}}/_{F_{cold}}) \times 10^3 \quad (1)$$

All measurements were conducted as $N = 3$ and the results were presented as mean values ± standard error of the mean (SEM). As previously described for MST data analysis,[31,33,34] the mean values of the aptamer DRN-10 were fitted to a fit function from law of mass action according to a 1:1 binding model to obtain the dissociation constant $K_D$ (Equation 2):

$$\Delta F_{norm}(c_L) = F_{UB} + (F_B - F_{UB})/2 \times (c_A + c_L + K_D - \sqrt{(c_A + c_L + K_D)^2 - 4 \times c_A \times c_L}) \quad (2)$$

where $c_L$ is the ligand concentration, $c_A$ is the aptamer concentration, $F_{UB}$ is the normalised fluorescence under unbound conditions and $F_B$ is the normalised fluorescence under bond conditions. However, the data from the shortened aptamer DRN-10v were fitted to the Hill equation to obtain $EC_{50}$, the ligand concentration occupying half of the binding sites, which is the apparent dissociation constant (Equation 3). Here, the Hill coefficient $n$ describes the cooperativity of the binding events:

$$\Delta F_{norm}(c_L) = F_{UB} + (F_B - F_{UB}) \times \left(1 + (EC_{50}/c_L)^n\right)^{-1} \quad (3)$$

#### Surface plasmon resonance spectroscopy

The SPR measurements were performed using a four channel Biacore T200 (T100 upgraded) device controlled by the Biacore T200 control software vers. 2.0 (GE Healthcare Europe, Freiburg, Germany). All experiments were performed at 25 °C. The ligands DRN and DOX were immobilised by amine coupling on a chip surface containing carboxylic acid groups (G-COOH SensEye®, Ssens, Enschede, Netherlands). Immobilisation was performed in SPR running buffer HBS-P using a flow rate of 5-10 µL/min. Chip surface was conditioned with 200 µL 50 mM NaCl, 50 mM HCl and activated with 35 µL 0.02 M 1-ethyl-3-(3-dimethylaminopropyl)-carbodiimide and 0.05 M N-hydroxy-succinimide. Each ligand solution was injected until up to 50 response units (RU) were immobilised. Then, the surface was blocked with 35 µL 1 M ethanolamine (pH 8.5). An activated and blocked channel without ligand served as reference.

Binding analysis was conducted at a flow rate of 20 µL/min in aptamer binding buffer (except for 0.0005% (v/v) Tween 20) as running buffer. Up to 11 different concentrations of oligonucleotides in a range of 5 nM - 8 µM were injected with 120-s injections and a 300-s delay, followed by a 5-s washing step. After each oligonucleotide injection, the chip surface was regenerated by injection of 20 µL 50 mM $Na_2CO_3$ in a 1-min pulse. Measurements were conducted as $N = 2$-3. For proofing the two-state reaction model, solutions with 16 µM oligonucleotides were injected with injection times ranging from 60 s to 180 s with a constant flow rate of 5 µL/min, in order to achieve saturated association curves.[35,36]

For background correction, each response signal was adjusted by subtraction of the reference cell signal as well as by subtraction of adjusted buffer injection signals. Association and dissociation rates and constants were determined by using BIAevaluation software vers. 3.01 (GE Healthcare Europe). Data was analysed using a two-state reaction model, since fitting by a simple 1:1 interaction model (Langmuir binding) did not lead to satisfied results. The two-state model describes a 1:1 binding of the injected analyte *A* and the immobilised ligand *B* followed by a conformational change of the complex *AB* to the more stable complex *AB** as described in the Equations (4) and (5):

$$A + B \underset{k_{d1}}{\overset{k_{a1}}{\rightleftarrows}} AB \underset{k_{d2}}{\overset{k_{a2}}{\rightleftarrows}} AB^* \quad (4)$$

$$K_D = \frac{k_{d1}}{k_{a1}} \times \frac{k_{d2}}{k_{d2} + k_{a2}} \quad (5)$$

where $k_a$ and $k_d$ are the association/forward and dissociation/reverse rate constants of the binding reaction 1 and the conformational change reaction 2, respectively. Thus, $K_D$ is the overall equilibrium dissociation constant.[37]

In the SPR recordings, the signal *R* was related to the amount of the complex *AB* and $R_{max}$ was related to the initial amount of immobilised ligand *B* in the 1:1 binding model. Then, the association and dissociation phases of the sensorgrams of the two-state reaction model could be globally fitted to Equation (6) and Equation (7), respectively, with $n = 2$ und $R_n$ being the signal at the start of the dissociation:[38]

$$R = \sum_1^n (R_{max} \times [A])/(K_D + [A]) \times \left[1 - e^{-(k_{an} \times [A] + k_{dn})t}\right] \quad (6)$$

$$R = \sum_1^n R_n \times e^{-k_{dn} \times t} \quad (7)$$

Data fitting relied on the Marquardt-Levenberg algorithm and fitting quality was estimated from reduced $\chi^2$-values representing the ratio of the sum of squared differences between the fitted data ($r_f$) and experimental data ($r_x$) at each point and difference of data point numbers ($n$) and number of degrees of freedom ($p$):

$$\chi^2 = \sum_1^n (r_f - r_x)^2/(n - p) \quad (8)$$

$\chi^2$-values should be ideally in the same order of magnitude as the noise expressed as RU (typically <2) and not larger than 10% of the maximal response value ($R_{max}$) in a fitting process.

#### Circular dichroism spectroscopy

CD spectra were obtained with a Jasco-815 spectropolarimeter (Jasco Instruments, Gross-Umstadt, Germany) in a quartz cell with an optical path length of 1 mm. Aptamers were measured in different buffer solutions as indicated. Spectra were taken at room temperature (approx. 22 °C) in a wavelength range of 200 nm - 310 nm with a slit width of 1 nm. CD spectra were accumulated from three runs.

View Article Online
DOI: 10.1039/C9AN01347H



## Results and discussion

### Microscale thermophoresis

MST allows for quantitative analysis of the interaction between the anthracyclines and the oligonucleotides in free solution. For this, the concentration of the Cy5-labeled oligonucleotides was kept constant, whereas the anthracycline concentration was varied. In order to study the specificity of the aptamer DRN-10 with MST recordings, a set of four chemotherapeutic and antibiotic substances was tested (chemical structures shown in Figure S1 of the ESI†). The only difference between daunorubicin and doxorubicin is that the side chain at C14 of daunorubicin terminates with a methyl group, whereas that of doxorubicin terminates with a hydroxyl group. However, this slight structural difference leads to quite different areas of application in cancer treatment.[14]

Typical thermophoresis curves are shown in Figure 1. The analysis of the temperature jump and the thermophoresis effect resulted in the largest changes in $\Delta F_{norm}$ leading to more reliable data analysis as shown in Figure S2 of the ESI†. An increase in the daunorubicin concentration up to 100 nM resulted in an enhanced decrease in the fluorescence intensity (positive thermophoresis). This concentration regime indicates the aptamer-specific binding to daunorubicin. However, further increase in daunorubicin concentration up to 1 µM resulted in an opposing behaviour (negative thermophoresis). Indeed, daunorubicin is known for nonspecific intercalation into DNA with low affinity of approx. $2\times10^{-4}$ M for single-stranded DNA, inducing this opposing behaviour.[39]

From MST recordings, different binding properties could be observed for daunorubicin and doxorubicin to DRN-10 resulting in $K_D$-values of 4.3 nM ± 1.5 nM and 1.6 nM ± 0.5 nM (each $N$ = 3), respectively (Figure 1A). Thus, doxorubicin seems to bind slightly more efficiently to DRN-10 than daunorubicin, as previously reported by using competition fluorescence assays.[20] By introducing a hydroxyl group into the structure, an additional hydrogen bond interaction can improve the stabilisation of the aptamer-ligand-complex. On the other hand, the structurally more altered antibiotics tetracycline and chloramphenicol (see Figure S1 of the ESI†) showed no specific binding to DRN-10 (Figure 1A). At concentrations >100 nM unspecific intercalation could be seen for daunorubicin and doxorubicin and at even higher concentrations tetracycline and chloramphenicol trended also to show unspecific binding.

In addition to the full-length 80 nt aptamer DRN-10, a truncated version with 41 nt (DRN-10v) was tested. The core sequence of the truncated aptamer DRN-10v was still sufficient for specific binding to daunorubicin and doxorubicin, whereas no specific binding could be observed for chloramphenicol and tetracycline (Figure 1B). Interestingly, data fitting according to a 1:1 binding model was not feasible. In fact, data were fitted to the Hill equation yielding an apparent dissociation constant $EC_{50}$ and leading to Hill coefficients of $n$ = 2.5-2.6 indicating somehow positively cooperative binding.[41] Binding of daunorubicin and doxorubicin to DRN-10v resulted in $EC_{50}$-values of 1.3 nM ± 0.1 nM and 0.8 nM ± 0.1 nM (each $N$ = 3), respectively. The previously reported $K_D$-value for daunorubicin/DRN-10v of 272 nM from SPR recordings was significantly larger.[20] However, in this concentration regime the MST recordings compete against the visible unspecific intercalation of anthracyclines into the DNA aptamer as seen for concentrations >100 nM (Figure 1B). Indeed, in the daunorubicin and doxorubicin concentration range of 5-100 nM one could speculate about a slight decrease in $\Delta F_{norm}$-values probably indicating the lower binding affinity to DRN-10v, but this effect seems to be compensated more and more by an opposing trend due to unspecific intercalation. Moreover, compared to the positive thermophoresis effect during specific binding using the full-length DRN-10, the truncated DRN-10v resulted in a negative thermophoresis effect. Therefore, the molecule-solvent interface, to which

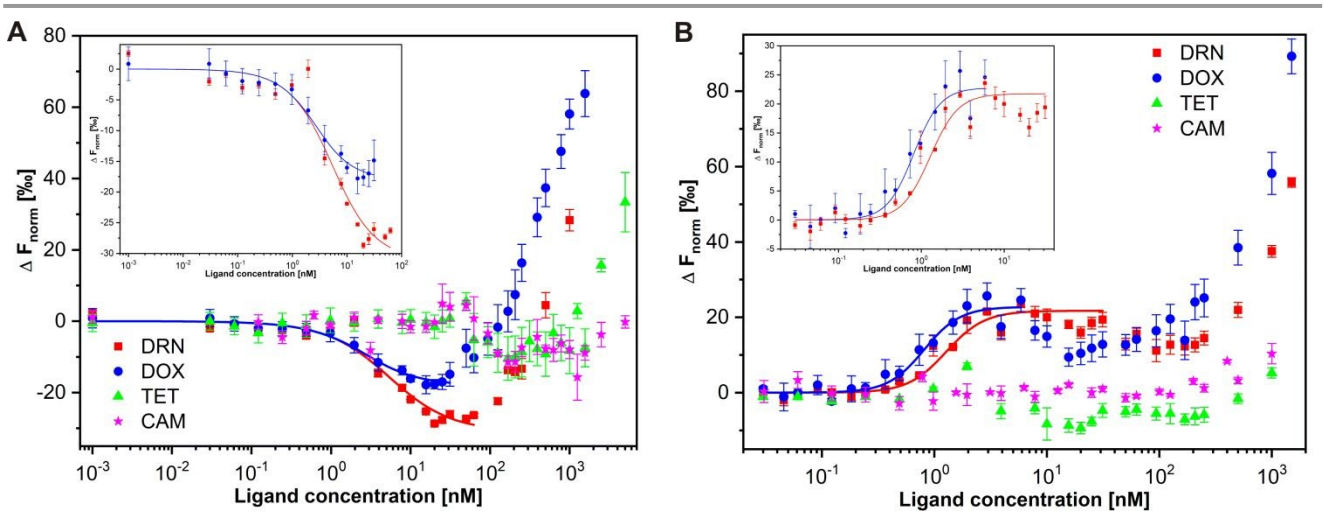


**Figure 1** Microscale thermophoresis (MST) data for binding analysis of **(A)** the aptamer DRN-10 and **(B)** the truncated version DRN-10v. Binding curves for aptamers and four antibiotics were analysed from T-jump and thermophoresis; means ± SEM, $N$ = 3. The ***insets*** show the concentration regimes of daunorubicin and doxorubicin for specific binding. The solid lines represent the fits of data to (A) the 1:1 binding model and (B) the Hill equation with the Hill coefficients being $n_{DRN}$ = 2.5 ± 0.3 and $n_{DOX}$ = 2.6 ± 0.8.



 

View Article Online
DOI: 10.1039/C9AN01247H



MST is sensitive, is very different for both systems. This could be an indication for a 3D-structural change of DRN-10v leading to an additional high-affinity binding step preceding a low-affinity binding step.

On the other hand, an 80 nt control DNA oligonucleotide (Con1) showed sequence similarities with the full-length aptamer DRN-10, but in the core sequence, several bases were substituted. Con1 exhibits G-quadruplex structures (see Figure 4), thought as prerequisite for binding, but neither daunorubicin nor doxorubicin showed specific binding to Con1. Only the unspecific intercalation at higher concentrations could be observed (Figure S3 of the ESI†).

In addition to MST, fluorescence correlation spectroscopy (FCS) also allows binding studies in free solution by recording fluorescence intensity fluctuations of daunorubicin. However, no significant changes in the diffusion time of daunorubicin could be observed during the interaction with DRN-10 as shown in Figure S4 of the ESI†. The low fluorescence signal of daunorubicin seems to require a larger daunorubicin/aptamer mass difference of a factor of >500 to resolve specific binding effects with FCS as postulated previously.[42] Thus, FCS recordings could be improved by coupling daunorubicin to a highly fluorescent label or by increasing the DRN-10 size significantly e.g. by coupling to PEG or dextrans.

**Surface plasmon resonance spectroscopy**

In contrast to MST, the SPR method allows normally a more detailed analysis of molecular interactions. SPR delivers also the association and dissociation constants ($K_A$ and $K_D$) of binding partners, but the additional analysis of kinetic parameters, consisting of the reaction rate constants of the association ($k_{on}$) and the dissociation ($k_{off}$), has made the SPR method to a gold standard in analysis of molecular interactions. However, SPR can be prone to incorrect coupling of ligands to the sensor surface or any unspecific binding on the sensor surface as well as to analytes with too small molecular masses. The last point has also defined the experimental conditions used here, since the small anthracyclines were immobilised instead of the oligonucleotides. This constellation has ensured well utilisable results. The low ligand density on the chip surface prevented rebinding of analyte molecules and mass transport effects. In addition, the use of natural binding partners without any modifications has significantly reduced the risk for a changed binding behaviour due to chemical modifications.

Analysis of the SPR sensorgrams of the specific DNA-aptamer DRN-10 and their two truncated versions DRN-10R and DRN-10v resulted in high binding affinities in the *nM*-range, whereas the two control oligonucleotides Con1 and Con2 did not exhibit any binding to the anthracyclines daunorubicin and doxorubicin (Figure 2A-E). The evaluation of the association and dissociation data curves was performed by a global fitting to a two-state reaction model according to Equation (4) with oligonucleotide concentrations in a range of 5 nM - 1 µM, since data fitting according to a 1:1 binding model did not result in sufficiently acceptable fitting curves and $\chi^2$-values. The $K_D$-values of the aptamers DRN-10 and DRN-10R to doxorubicin calculated from the kinetic data were very similar, yielding 11 nM and 26 nM, respectively. The $K_D$-values of DRN-10 and DRN-10R to daunorubicin were only slightly higher, yielding 22 nM and 27 nM. Despite exhibiting similar $K_D$-values, differences were observed in the kinetic data (see also Table 1). In the case of the aptamer-target complex building, the $k_{a1}$-values of the aptamers DRN-10 and DRN-10R to daunorubicin were determined to $1.6 \times 10^5$ $M^{-1}s^{-1}$ and $1.5 \times 10^5$ $M^{-1}s^{-1}$, being slightly higher than those for doxorubicin. On the other hand, the $k_{d1}$-values of DRN-10 and DRN-10R to daunorubicin were calculated to $3.3 \times 10^{-2}$ $s^{-1}$ and $3.0 \times 10^{-2}$ $s^{-1}$, being smaller than those for doxorubicin. The unravelled differences in the kinetic behaviour supported previous observations in a competitive fluorescence assay, in which a higher binding affinity of DRN-10 to doxorubicin than to daunorubicin has been recognised.[20] However, Wochner et al. have applied a simple 1:1 Langmuir binding model yielding a very similar $K_D$-value of 20 nM for DRN-10 to daunorubicin, based on a smaller $k_{on}$-value of $3.3 \times 10^4$ $M^{-1}s^{-1}$and smaller $k_{off}$-value of $6.5 \times 10^{-4}$ $s^{-1}$, but without information about the fitting quality except for a worse $\chi^2$-value of 2.95. The differences are most probably the result of altered SPR experimental conditions and varying binding models. Different anthracycline coupling procedures to the sensor surface (amine-coupling *vs*. streptavidin-biotin) as well as the different injection methods with varying concentration ranges could lead to altered binding affinities, even though studying the same aptamer-anthracycline system.

Recently, the truncated aptamer DRN-10R has been applied in an aptasensor for doxorubicin detection based on electrochemical impedance spectroscopy yielding an apparent $K_D$-value of 64 nM.[26] A Hill coefficient of $n = 3.4$ indicated positive cooperativity similar to the data shown here for the strongest truncated form DRN-10v in the MST recordings (see Figure 1B). However, the higher $K_D$-value could be partly due to the fact that an inverse experimental setup with aptamer surface immobilisation has been used.

The strongest truncated aptamer DRN-10v has shown significantly lower binding affinities with $K_D$-values of 144 nM to daunorubicin and 125 nM to doxorubicin. Again, in contrast to similar binding constants for both anthracyclines, significant differences in their binding kinetics could be unravelled (Figure 2F). Compared to the aptamers DRN-10 and DRN-10R, the $k_{a1}$-values of DRN-10v were 3-5-fold higher with $8.5 \times 10^5$ $M^{-1}s^{-1}$ for daunorubicin and $3.2 \times 10^5$ $M^{-1}s^{-1}$ for doxorubicin, but $k_{d1}$-values of DRN-10v were also 2-4-fold higher for both targets. Surprisingly, Wochner et al. have found an even higher $K_D$-value of 272 nM for DRN10v to daunorubicin, however, by applying again the simple 1:1 Langmuir binding model.[20]

View Article Online
DOI: 10.1039/C9AN01247H



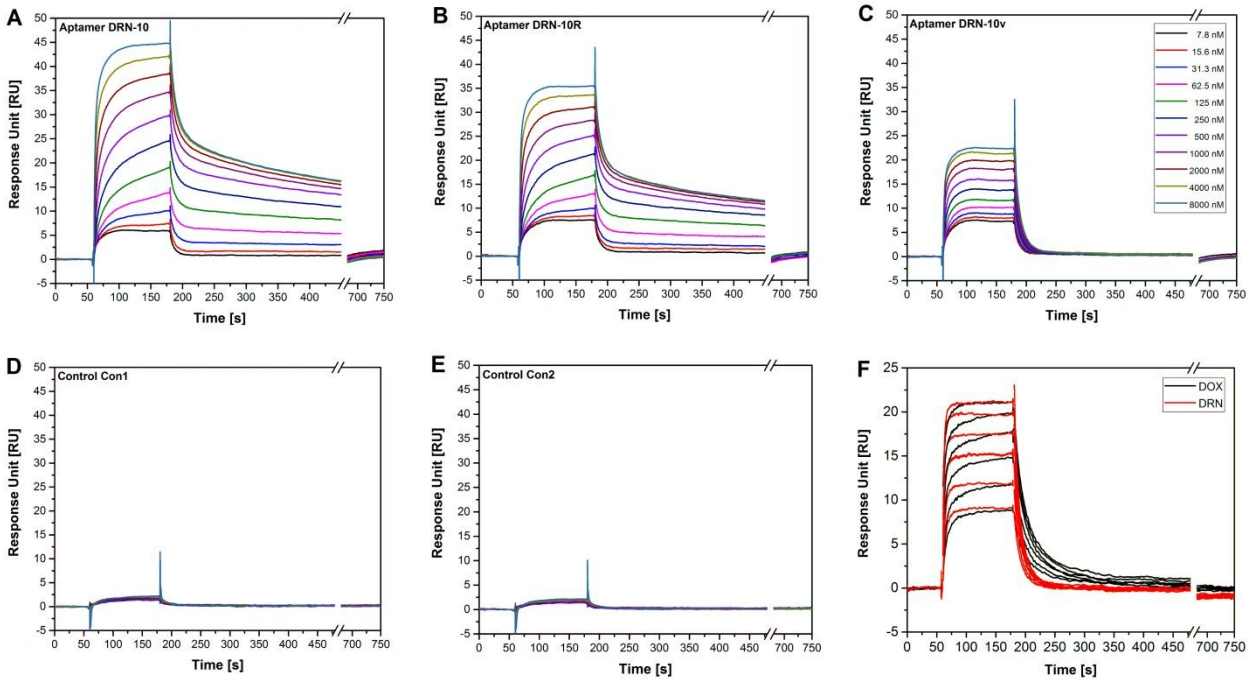


**Figure 2** Analysis of anthracycline/aptamer interactions by using surface plasmon resonance (SPR) spectroscopy. Sensorgrams of the binding behaviour of the aptamer (**A**) DRN-10, (**B**) DRN-10R, (**C**) DRN-10v, (**D**) Con1 and (**E**) Con2 to immobilised daunorubicin as a function of 11 varying aptamer concentrations (5 nM – 8 µM, as indicated in (C)). Each interaction is described by a 120 s association and 300 s dissociation curves. The 3 DRN-aptamers shown in A-C exhibit a strong interaction to the daunorubicin and the resulting curves could be globally fitted to a two-state reaction model. (**F**) Normalised sensorgrams of the bimolecular systems daunorubicin/DRN-10v (red) and the doxorubicin/DRN-10v (black), indicating the differences in the association and dissociation rate constants of the binding behaviour for the aptamer DRN-10v to the ligands.

The $\chi^2$-values of each fitting process applying a two-state reaction model resulted in values <1 and therefore <2% of the corresponding $R_{max}$-values and met very well the theoretical requirements. When applying the simple 1:1 Langmuir binding model, fitting data delivered similar $K_D$-values, but with significantly higher $\chi^2$-values ranging 2-5% of the corresponding $R_{max}$-values. Particularly, the fitting curves did not match the measuring curves during the dissociation phase, despite of optimisation by buffer jump or minimised ligand immobilisation.

Evidence for the two-state reaction model could be also achieved from an analyte binding test with different contact times between doxorubicin and DRN-10 (Figure 3A). By increasing the aptamer injection time (association time) from

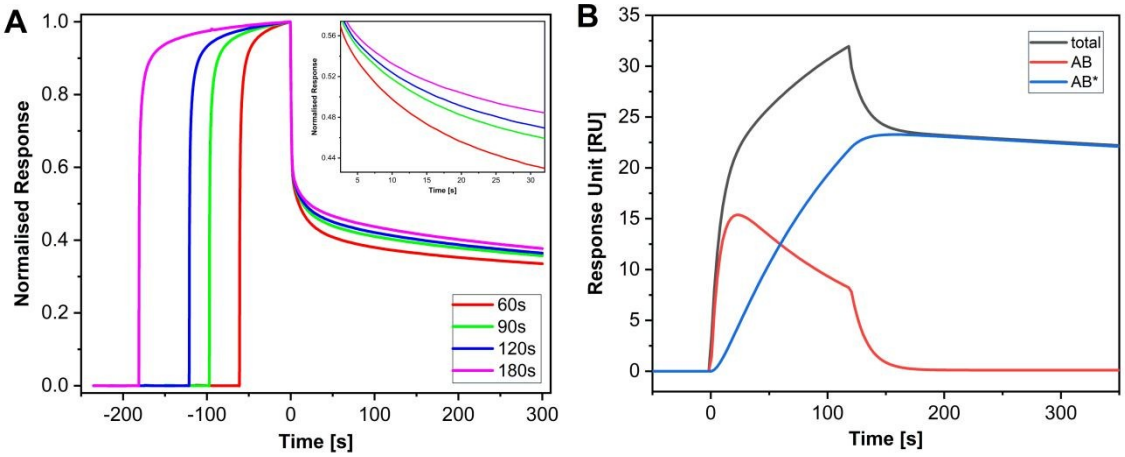


**Figure 3** Two-state reaction of doxorubicin with the aptamer DRN-10 as detected by SPR measurements. (**A**) Sensorgrams show the effect of increased injection time on the stability of the doxorubicin/DRN-10 complex. Measurements were performed for 16 µM aptamer solution with injection times of 60-180 s at a constant flow rate of 5 µL/min. For comparison, sensorgrams were normalised to $R_{max}$-values and aligned to endpoint of the injection phase. The ***inset*** shows the initial dissociation phase in an enlarged view. (**B**) Shown sensorgram is obtained for 500 nM DRN-10 with 120 s injection time at 20 µL/min and was fitted to the two-state reaction model. The experimental response (grey line) is the sum of the initial binding (AB, red line) and the subsequent conformational change (AB*, blue line).

View Article Online
DOI: 10.1039/C9AN01247H



60 s to 180 s, one would expect an increased amount of the conformational change following the preceding aptamer-anthracycline binding (*AB*). This would lead to an accumulation of the more stable complex (*AB**), but also to longer dissociation phases. Indeed, elongated dissociation phases were observed when increasing the association times (Figure 3A, *inset*). This was also true for DRN-10 interaction with daunorubicin. In addition, the deconvolution of the experimental data revealed that at first the aptamer-anthracycline binding complex *AB* is formed rapidly. Then, the stable complex *AB** appeared delayed more slowly (Figure 3B).

However, the structure of single-stranded nucleic acids is highly complex with many degrees of freedom and it is very likely that the formation of an aptamer-target binding complex is connected with one or more conformational changes in the nucleic acid structure. The results of CD spectroscopic recordings (see below, Figure 4) seem to confirm this assumption. However, further analyses will be necessary for proofing the hypothesis of a more complex binding model. This could be conducted by several spectroscopic techniques such as nuclear magnetic resonance spectroscopy or X-ray crystallography.[43]

### Circular dichroism spectroscopy

For 3D structure stability and recognition properties of aptamers, guanine quadruplex structures (G-quadruplexes) are highly important.[44] Oligonucleotides with a G-rich sequence as also true for DRN-10 and its derivatives can form G-quadruplexes. In order to correlate the different binding affinities of anthracyclines to the structure of the varied aptamers, CD spectra were obtained since they can provide reliable information about the G-quadruplex formation.[45,46] In Figure 4A, CD spectra of all used DNA oligonucleotides in aptamer buffer are shown. For both the aptamers DRN-10 and DRN-10v and the control Con1, absorption maxima at 210 nm and 265 nm as well as minima at 240 nm could be observed. In general, this is a typical feature for parallel DNA quadruplexes. These aptamers also exhibited positive shoulders at 295 nm indicating unimolecular or bimolecular parallel DNA quadruplex structure with external loops rather than a tetramolecular parallel DNA quadruplex.[44,45,47] On the other hand, for the control Con2 the relevant peaks at 210 nm, 240 nm and 265 nm were shifted to longer wavelengths and in addition, a prominent shoulder at 295 nm was missing. Thus, Con2 seemed not to form a quadruplex structure.

Upon binding to daunorubicin, an additional conformational change could be observed for the aptamers DRN-10 and DRN-10v (Figure 4B) as already shown for other aptamers.[48] In fact, the maximum at 265 nm was red-shifted, whereas the minimum at 240 nm was slightly blue-shifted, however, the 3D structure seemed still to be a G-quadruplex. The suggested two-state reaction model from analysed SPR recordings including a conformational change after aptamer-anthracycline-binding underlines this observation (see Figure 3). This observation could probably also explain the 10-100× higher dissociation constants obtained with SPR in comparison to that from MST. Due to the immobilisation of anthracyclines for SPR recordings, the conformational change required for successful binding to aptamer could be somehow hindered. This hindrance seemed to be more pronounced for the truncated aptamer as one would expect for a less expanded binding partner. Indeed, several groups have shown that SPR recordings match MST recordings.[49–51] However, the reliability of dissociation constants determined from immobilised binding partners is still debated.[52] Therefore, restrictions in rotational freedom and diffusion properties of the binding partners can lead to altered binding characteristics.

CD recordings for the aptamers and controls were also performed under different ionic conditions (Figure 5A-D), since quadruplex formation requires the presence of monovalent cations, in particular $Na^+$ and $K^+$.[53] When removing monovalent and/or divalent cations from the buffer solution, almost no changes in CD spectra could be observed for Con2 (Figure 5D), indicating the absence of an ion-dependent 3D-structural formation as expected from the nucleotide sequence. For the aptamers DRN-10, DRN-10v

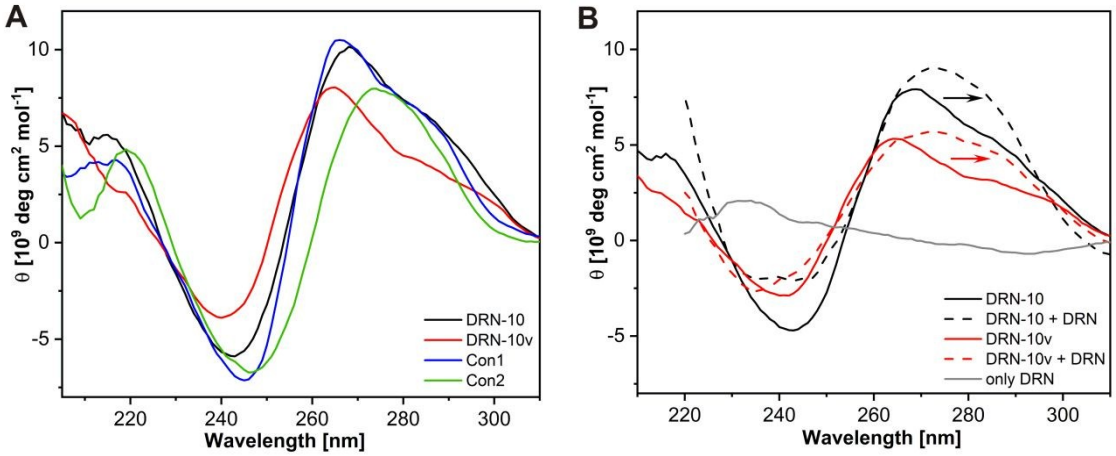


**Figure 4** CD spectra of the investigated DNA oligonucleotides. (**A**) Comparison of the CD spectra of the oligonucleotides (c = 15 µM) in aptamer buffer. (**B**) Effect of the absence (solid lines) or presence (dashed lines) of 200 µM daunorubicin on the CD spectra of the aptamers DRN-10 and DRN-10v (c = 15 µM). The CD spectrum of daunorubicin alone is shown for comparison. Due to strong absorbance of daunorubicin <200 nm, these data points were discarded.

View Article Online
DOI: 10.1039/C9AN01247H

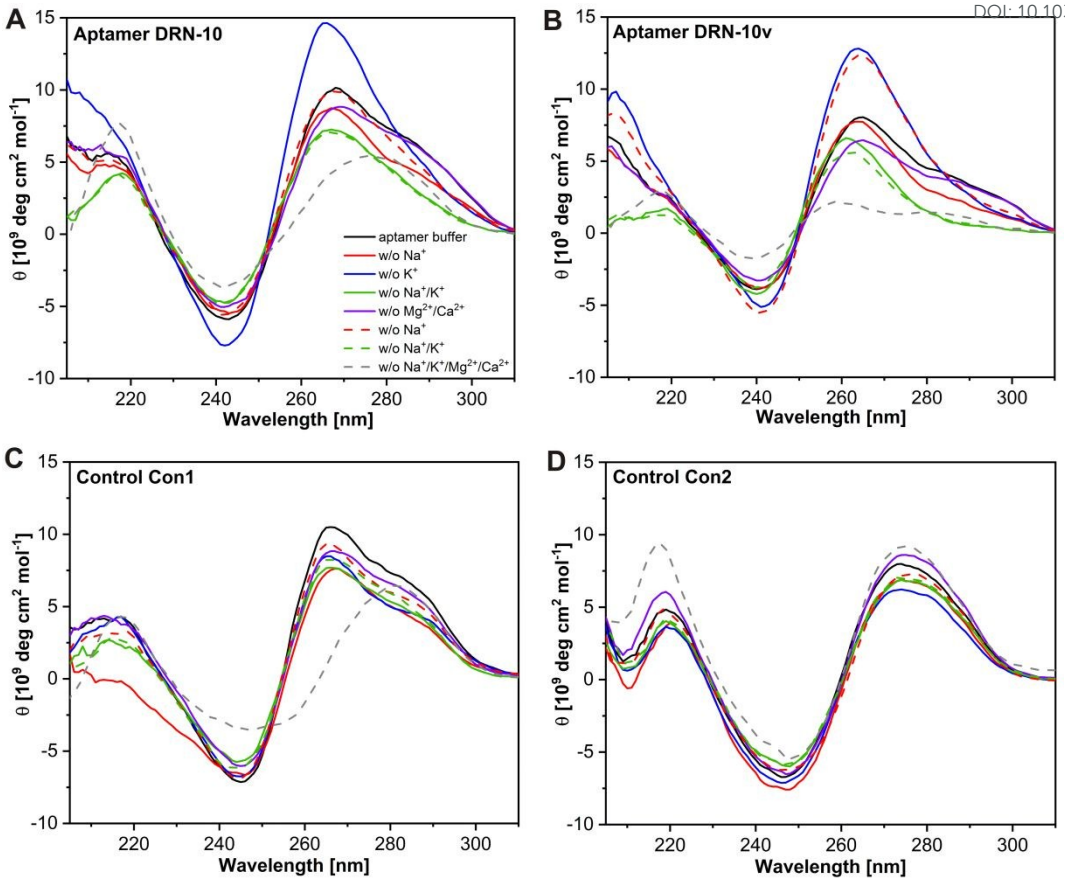


**Figure 5** CD spectra of the studied oligonucleotides. **(A-D)** Effect of different buffer conditions as indicated in (A). Solid lines denote buffer conditions, in which ionic strength was kept constant by substituting with appropriate amounts of choline chloride. Dashed lines denote buffer conditions without compensating with choline chloride.

and Con1, significant changes in CD spectra were visible under different ionic conditions. However, the compensation of the ionic strength had not that much influence (Figure 5A-C, compare green and red solid *vs*. dashed lines). Combined removal of $Ca^{2+}/Mg^{2+}$ did not change the CD spectral pattern compared to the aptamer buffer. Removal of $Na^+$ or $K^+$ resulted in a diminished shoulder at 295 nm, and this effect was even stronger for combined removal of $Na^+/K^+$, then also changing the pattern at 210 nm. Finally, the combined removal of $Na^+/K^+/Mg^{2+}/Ca^{2+}$ led to a total change in the CD spectral pattern (as was not the case for Con2). This observation fits to previous results from fluorescence binding assays, even though a larger influence of $Na^+$ removal on binding properties has been detected.[20] It can be concluded from the CD results that a quadruplex formation seems to be the 3D-structural basis for specific binding, although the quadruplex formation alone is not sufficient as shown for Con1. Moreover, the quadruplex formation is not predominantly dependent on one of the four tested cations. This fact is quite contrary to the general opinion that quadruplex formation requires especially monovalent cations. However, in general bimolecular quadruplexes appear not to be markedly dependent on the nature of the cation, in striking contrast with unimolecular quadruplexes.[54]

## Conclusions

The comprehensive analysis of the binding behaviour of recognition elements to their targets is very important for the intended application. Here, we could demonstrate that MST and SPR could be used to reliably measure the binding affinities of small antibiotics to DNA aptamers, whereas FCS failed due to insufficient mass changes. The obtained data are summarised in Table 1. Thus, the DNA aptamer DRN-10 is a very promising recognition element for reliable and sensitive daunorubicin and doxorubicin detection systems.

From the experiments, it turned out that for the anthracyclines daunorubicin and doxorubicin similar $K_D$-values in the *nM*-range could be determined, although method-dependent differences were unravelled. From CD recordings, a specific G-quadruplex could be suggested as structural basis for anthracycline binding. Thus, the 3D conformational changes upon anthracycline binding could be somehow hindered when studying an immobilised partner. As this is the case for the SPR recordings, higher $K_D$-values would be reasonable. In this view, the weaker apparent binding obtained from SPR nicely correlates to the stronger truncation of the aptamer. However, MST recordings indicated the still existing specific binding of even strongest truncated aptamer.

View Article Online
DOI: 10.1039/C9AN01247H

**Table 1** Comparison of determined binding affinity data from SPR and MST recordings.

| | Aptamer | DRN-10 | | DRN-10R | | DRN-10v | |
|---|---|---|---|---|---|---|---|
| | Anthracycline * | DRN | DOX | DRN | DOX | DRN | DOX |
| SPR | $k_{a1}$ [$M^{-1}$ $s^{-1}$] | $1.6 \times 10^5$ | $1.2 \times 10^5$ | $1.5 \times 10^5$ | $1.0 \times 10^5$ | $8.5 \times 10^5$ | $3.2 \times 10^5$ |
| | $k_{d1}$ [$s^{-1}$] | $3.3 \times 10^{-2}$ | $6.2 \times 10^{-2}$ | $3.0 \times 10^{-2}$ | $3.5 \times 10^{-2}$ | $1.4 \times 10^{-1}$ | $6.2 \times 10^{-2}$ |
| | $k_{a2}$ [$s^{-1}$] | $1.2 \times 10^{-2}$ | $1.6 \times 10^{-2}$ | $1.2 \times 10^{-2}$ | $1.5 \times 10^{-2}$ | $3.2 \times 10^{-4}$ | $1.9 \times 10^{-3}$ |
| | $k_{d2}$ [$s^{-1}$] | $1.4 \times 10^{-3}$ | $3.6 \times 10^{-4}$ | $1.8 \times 10^{-3}$ | $1.1 \times 10^{-3}$ | $2.9 \times 10^{-3}$ | $3.3 \times 10^{-3}$ |
| | $K_D$ [nM] | 22 | 11 | 27 | 26 | 144 | 125 |
| | $\chi^2$ | 0.35 | 0.65 | 0.13 | 0.20 | 0.09 | 0.13 |
| MST | $K_D$ [nM] | 4.3 | 1.6 | n.d. | n.d. | n/a | n/a |
| | $EC_{50}$ [nM] | n/a | n/a | n.d. | n.d. | 1.3 | 0.8 |
| | $n$ | 1.0 | 1.0 | n.d. | n.d. | 2.5 | 2.6 |

* DRN daunorubicin, DOX doxorubicin; n/a not appropriate; n.d. not determined

Thus, the combination of different analysis methods allows for a more reliable estimation of the true binding behaviour. The combination of MST and SPR seems to be a very powerful tool. In addition to $K_D$-values, from SPR more complex binding kinetics can be obtained, whereas MST allows for rapid screening under more physiological conditions.

## Conflicts of interest

There are no conflicts to declare.

## Acknowledgements

We thank Anja Thalhammer (Physical Biochemistry group, University of Potsdam) for supporting us with the CD spectroscopic recordings.

This work was supported by the German Federal Ministry of Education and Research BMBF within the funding program InnoProfile-Transfer [grant number 03IPT517Y to C.H.]; within the funding program Photonics Research Germany [grant number 13N13777 to C.H.]; and by the German Federal Ministry for Economic Affairs and Energy BMWi within the Central Innovation Programme [grant number ZF4086507MD6 to M.M.].

## References

1 B. Alberts, A. Johnson, J. Lewis, D. Morgan, M. Raff, K. Roberts and P. Walter, *Molecular Biology of the Cell*, Garland Science, New York, 6th edn., 2014.
2 C. I. L. Justino, A. C. Freitas, R. Pereira, A. C. Duarte and T. A. P. Rocha Santos, *TrAC Trends Anal. Chem.*, 2015, **68**, 2–17.
3 M. Zhou, Q. Li and R. Wang, *ChemMedChem*, 2016, **11**, 738–756.
4 A. M. Rossi and C. W. Taylor, *Nat. Protoc.*, 2011, **6**, 365–387.
5 A. G. Ngounou Wetie, I. Sokolowska, A. G. Woods, U. Roy, J. A. Loo and C. C. Darie, *Proteomics*, 2013, **13**, 538–557.
6 C. M. Santiveri, B. López-Méndez, S. Huecas, C. Alfonso, J. R. Luque-Ortega, R. Campos-Olivas, C. M. Santiveri, B. López-Méndez, S. Huecas, C. Alfonso, J. R. Luque-Ortega and R. Campos-Olivas, in *eLS*, John Wiley & Sons, Ltd, Chichester, UK, 2017, pp. 1–16.
7 A. D. Ellington and J. W. Szostak, *Nature*, 1990, **346**, 818–822.
8 D. L. Robertson and G. F. Joyce, *Nature*, 1990, **344**, 467–468.
9 C. Tuerk and L. Gold, *Science*, 1990, **249**, 505–10.
10 M. Menger, A. Yarman, J. Erdőssy, H. Yildiz, R. Gyurcsányi and F. Scheller, *Biosensors*, 2016, **6**, 35.
11 K.-M. Song, S. Lee and C. Ban, *Sensors*, 2012, **12**, 612–631.
12 A. B. Iliuk, L. Hu and W. A. Tao, *Anal. Chem.*, 2011, **83**, 4440–4452.
13 M. Jing and M. T. Bowser, *Anal. Chim. Acta*, 2011, **686**, 9–18.
14 G. Minotti, P. Menna, E. Salvatorelli, G. Cairo and L. Gianni, *Pharmacol. Rev.*, 2004, **56**, 185–229.
15 P. Pophali and M. Litzow, *Curr. Treat. Options Oncol.*, 2017, **18**, 3.
16 U. Creutzig, S. Diekamp, M. Zimmermann and D. Reinhardt, *Pediatr. Blood Cancer*, 2007, **48**, 651–662.
17 L. Dai, J. Liu, Z. Luo, M. Li, K. Cai, A. Burns, D. J. Kornbrust, M. E. Davis, A. Rait, E. H. Chang, J. H. Li, K. Y. Cai and Y. L. Zhao, *J. Mater. Chem. B*, 2016, **4**, 6758–6772.
18 Y. Zhang, H. Hong and W. Cai, *Curr. Med. Chem.*, 2011, **18**, 4185–94.
19 N. M. Danesh, P. Lavaee, M. Ramezani, K. Abnous and S. M. Taghdisi, *Int. J. Pharm.*, 2015, **489**, 311–317.
20 A. Wochner, M. Menger, D. Orgel, B. Cech, M. Rimmele, V. A. Erdmann and J. Glökler, *Anal. Biochem.*, 2008, **373**, 34–42.
21 B. Doughty, Y. Rao, S. W. Kazer, S. J. J. Kwok, N. J. Turro and K. B. Eisenthal, *J. Phys. Chem. B*, 2013, **117**, 15285–15289.
22 Y. J. Schneider, R. Baurain, A. Zenebergh and A. Trouet, *Cancer Chemother. Pharmacol.*, 1979, **2**, 7–10.
23 A. J. Simon, A. Vallée-Bélisle, F. Ricci and K. W. Plaxco, *Proc. Natl. Acad. Sci. U. S. A.*, 2014, **111**, 15048–53.
24 K. Plourde, R. M. Derbali, A. Desrosiers, C. Dubath, A. Vallée-Bélisle and J. Leblond, *J. Control. Release*, 2017, **251**, 82–91.
25 N. Omar, Q. Loh, G. Tye, Y. Choong, R. Noordin, J. Glökler, T. Lim, N. Omar, Q. Loh, G. J. Tye, Y. S. Choong, R. Noordin, J. Glökler and T. S. Lim, *Sensors*,

2013, **14**, 346–355.
26 N. Bahner, P. Reich, D. Frense, M. Menger, K. Schieke and D. Beckmann, *Anal. Bioanal. Chem.*, 2018, **410**, 1453–1462.
27 P. Chandra, H.-B. Noh, M.-S. Won and Y.-B. Shim, *Biosens. Bioelectron.*, 2011, **26**, 4442–4449.
28 B. S. Ferguson, D. A. Hoggarth, D. Maliniak, K. Ploense, R. J. White, N. Woodward, K. Hsieh, A. J. Bonham, M. Eisenstein, T. E. Kippin, K. W. Plaxco and H. T. Soh, *Sci. Transl. Med.*, 2013, **5**, 213ra165.
29 N. Arroyo-Currás, J. Somerson, P. A. Vieira, K. L. Ploense, T. E. Kippin and K. W. Plaxco, *Proc. Natl. Acad. Sci. U. S. A.*, 2017, **114**, 645–650.
30 X. Guo, *J. Biophotonics*, 2012, **5**, 483–501.
31 C. Entzian and T. Schubert, *Methods*, 2016, **97**, 27–34.
32 S. A. I. Seidel, P. M. Dijkman, W. A. Lea, G. van den Bogaart, M. Jerabek-Willemsen, A. Lazic, J. S. Joseph, P. Srinivasan, P. Baaske, A. Simeonov, I. Katritch, F. A. Melo, J. E. Ladbury, G. Schreiber, A. Watts, D. Braun and S. Duhr, *Methods*, 2013, **59**, 301–315.
33 D. Breitsprecher, N. Schlinck, D. Witte, S. Duhr, P. Baaske and T. Schubert, in *Methods in molecular biology (Clifton, N.J.)*, 2016, vol. 1380, pp. 99–111.
34 M. Jerabek-Willemsen, T. André, R. Wanner, H. M. Roth, S. Duhr, P. Baaske and D. Breitsprecher, *J. Mol. Struct.*, 2014, **1077**, 101–113.
35 P. Murat, D. Cressend, N. Spinelli, A. Van der Heyden, P. Labbé, P. Dumy and E. Defrancq, *ChemBioChem*, 2008, **9**, 2588–2591.
36 R. L. Rich and D. G. Myszka, *J. Mol. Recognit.*, 2009, **23**, 1–64.
37 *Biacore T200 Software Handbook 28-9768-78 Edition AA*, Uppsala, Sweden, 2010.
38 T. A. Morton, D. G. Myszka and I. M. Chaiken, *Anal. Biochem.*, 1995, **227**, 176–185.
39 C. Gui-Fang, Z. Jie, T. Yong-Hua, H. Pin-Gang and F. Yu-Zhi, *Chinese J. Chem.*, 2005, **23**, 576–580.
40 V. J. B. Ruigrok, M. Levisson, J. Hekelaar, H. Smidt, B. W. Dijkstra and J. van der Oost, *Int. J. Mol. Sci.*, 2012, **13**, 10537–52.
41 J. N. Weiss, *FASEB J.*, 1997, **11**, 835–41.
42 U. Meseth, T. Wohland, R. Rigler and H. Vogel, *Biophys. J.*, 1999, **76**, 1619–31.
43 E. Muñoz, D. Xu, M. Kemp, F. Zhang, J. Liu and R. J. Linhardt, *Biochemistry*, 2006, **45**, 5122–5128.
44 V. Viglasky and T. Hianik, *Gen. Physiol. Biophys.*, 2013, **32**, 149–172.
45 M. Małgowska, D. Gudanis, A. Teubert, G. Dominiak and Z. Gdaniec, *BioTechnologia*, 2012, **4**, 381–390.
46 M. Vorlíčková, I. Kejnovská, J. Sagi, D. Renčiuk, K. Bednářová, J. Motlová and J. Kypr, *Methods*, 2012, **57**, 64–75.
47 M. Vorlíčková, I. Kejnovská, K. Bednářová, D. Renčiuk and J. Kypr, *Chirality*, 2012, **24**, 691–698.
48 P.-H. Lin, R.-H. Chen, C.-H. Lee, Y. Chang, C.-S. Chen and W.-Y. Chen, *Colloids Surfaces B Biointerfaces*, 2011, **88**, 552–558.
49 T. Rogez-Florent, C. Foulon, A.-S. Drucbert, N. Schifano, P. Six, S. Devassine, P. Depreux, P.-M. Danzé, L. Goossens, C. Danel and J.-F. Goossens, *J. Pharm. Biomed. Anal.*, 2017, **137**, 113–122.
50 C. Seeger, V. O. Talibov and U. H. Danielson, *J. Mol. Recognit.*, 2017, **30**, e2621.
51 M. Ramakrishnan, F. Alves De Melo, B. M. Kinsey, J. E. Ladbury, T. R. Kosten and F. M. Orson, *PLoS One*, 2012, **7**, e40518.
52 D. G. Myszka, *Curr. Opin. Biotechnol.*, 1997, **8**, 50–57.
53 S. Paramasivan, I. Rujan and P. H. Bolton, *Methods*, 2007, **43**, 324–331.
54 S. Burge, G. N. Parkinson, P. Hazel, A. K. Todd and S. Neidle, *Nucleic Acids Res.*, 2006, **34**, 5402–5415.

View Article Online
DOI: 10.1039/C9AN01247H

**Graphical abstract**

A combined methodological approach supports a two-state reaction model including a 1:1 binding of anthracyclines and aptamers and a subsequent conformational change of the binding complex.